

# Geometrical Principles of Homomeric $\beta$ -barrels and $\beta$ -helices: Application to Modelling Amyloid Protofilaments

Steven Hayward<sup>1</sup> and E. James Milner-White<sup>2</sup>

<sup>1</sup> D'Arcy Thompson Centre for Computational Biology, School of Computing Sciences,  
University of East Anglia, Norwich, NR4 7TJ, UK

<sup>2</sup> College of Medical, Veterinary and Life Sciences, University of Glasgow, Glasgow, G12  
8QQ, UK

**Contact:** Dr Steven Hayward, School of Computing Sciences, University of East Anglia,  
Norwich, NR4 7TJ, U.K. Tel: +44-1603-593542, Fax: +44-1603-593345, E-mail:  
[sjh@cmp.uea.ac.uk](mailto:sjh@cmp.uea.ac.uk)

**Running title:** Geometry of  $\beta$ -barrels and  $\beta$ -helices

**Keywords:** register shift, shear number, nanotube design, HET-s prion, Alzheimer's fibril

This article has been accepted for publication and undergone full peer review but has not been through the copyediting, typesetting, pagination and proofreading process which may lead to differences between this version and the Version of Record. Please cite this article as an 'Accepted Article', doi: 10.1002/prot.25341

© 2017 Wiley Periodicals, Inc.

Received: Apr 11, 2017; Revised: Jun 13, 2017; Accepted: Jun 21, 2017

**ABSTRACT**

Examples of homomeric  $\beta$ -helices and  $\beta$ -barrels have recently emerged. Here we generalise the theory for the shear number in  $\beta$ -barrels to encompass  $\beta$ -helices and homomeric structures. We introduce the concept of the “ $\beta$ -strip”, the set of parallel or antiparallel neighbouring strands, from which the whole helix can be generated giving it  $n$ -fold rotational symmetry. In this context the shear number is interpreted as the sum around the helix of the fixed register shift between neighbouring identical  $\beta$ -strips. Using this approach we have derived relationships between helical width, pitch, angle between strand direction and helical axis, mass per length, register shift, and number of strands. The validity and unifying power of the method is demonstrated with known structures including  $\alpha$ -haemolysin, T4 phage spike, cylindrin, and the HET-s(218-289) prion. From reported dimensions measured by X-ray fibre diffraction on amyloid fibrils the relationships can be used to predict the register shift and the number of strands within amyloid protofilaments. This was used to construct models of transthyretin and Alzheimer  $\beta$ (40) amyloid protofilaments that comprise a single strip of in-register  $\beta$ -strands folded into a “ $\beta$ -strip helix”. Results suggest both stabilisation of an individual  $\beta$ -strip helix as well as growth by addition of further  $\beta$ -strip helices involves the same pair of sequence segments associating with  $\beta$ -sheet hydrogen bonding at the same register shift. This association would be aided by a repeat sequence. Hence understanding of how the register shift (as the distance between repeat sequences) relates to helical dimensions, will be useful for nanotube design.

## INTRODUCTION

There are two main structural categories of helical structures within proteins that have  $\beta$ -sheet hydrogen bonding:  $\beta$ -barrels and  $\beta$ -helices.  $\beta$ -helices<sup>1</sup> (also called  $\beta$ -solenoids<sup>2</sup>) are parallel  $\beta$ -structures that are tightly wound with a packed interior. They often comprise just a single strand that maintains a direction approximately perpendicular to the helical axis. They can be both left-handed and right-handed and have various cross-sectional shapes, but are never circular comprising short stretches of largely straight  $\beta$ -strand with intervening loops where significant changes in chain direction occur. A classic example is the  $\beta$ -helix from pectin lyase<sup>3</sup>.  $\beta$ -barrels can be both parallel or antiparallel  $\beta$ -structures and are distinguishable from  $\beta$ -helices by comprising strands more aligned to the helical axis. This means, in contrast to the  $\beta$ -helix, the rise per turn is comparatively long and the strands complete only a fraction of a turn. They are often circular in cross-section and are always right-handed. An early classic example is the  $\alpha/\beta$ -barrel in the enzyme triosephosphate isomerase<sup>4</sup> a comparatively small structure which contrasts with the wider transmembrane  $\beta$ -barrels<sup>5,6</sup>.

McLachlan<sup>7</sup> introduced the concept of the shear number in  $\beta$ -barrels. It was elaborated upon later by Murzin et al<sup>8</sup>. It is a positive integer equal to the shift in number of residues along a strand when one follows the path of aligned residues around the  $\beta$ -barrel until one returns to the same strand. These authors showed that specifying the shear number and the number of strands forming a  $\beta$ -barrel specifies its helical geometry. Thus shear number and the number of strands is used by the Structural Classification of Proteins (SCOP) data base<sup>9</sup> to help classify  $\beta$ -barrels. The development of the theory for the shear number was tailored specifically to the  $\beta$ -barrel structure and applied in the context of a single subunit, i.e. for a non-symmetric structure.

Since the development of the shear number theory more  $\beta$ -helix structures have become available. Also, relatively recently, homomeric  $\beta$ -barrel and  $\beta$ -helix structures have been solved which display  $n$ -fold rotational symmetry about the helical axis. Thus there exists the opportunity to develop the shear number theory to encompass these structures. For convenience we use the terms nanotube or multi-strand helix to refer to any kind of  $\beta$ -barrel or  $\beta$ -helix.

In homomeric multi-strand helices with perfect  $n$ -fold rotational symmetry, the unit from which the whole structure can be constructed via symmetry operations, often consists of a group of strands rather than one. We name such a group of strands a “ $\beta$ -strip”. Here we show that in a number of well-known examples in both  $\beta$ -barrels and  $\beta$ -helices the symmetrical arrangement imposes a fixed register shift between  $\beta$ -strips which means that the shear number can be interpreted as a sum of register shifts between neighbouring identical  $\beta$ -strips around the multi-strand helix. The focus of our work is to develop comprehensive equations for such arrangements, explore the structural possibilities and apply them to the various multi-strand helices occurring in proteins with known 3-dimensional structures. We will show how a single graph encompasses all possible structures including  $\beta$ -barrels as well as  $\beta$ -helices.

The main motivation behind this work is to model the amyloid protofilament structure. Amyloid is the name given for an alternative protein conformation that the majority of proteins seem able to adopt, given appropriate conditions<sup>10</sup>. The process of amyloid formation damages cells and this is the underlying cause of several common diseases<sup>11,12</sup> including Alzheimer's, Parkinson's and type II diabetes. The infectious forms of prion

proteins<sup>13</sup> are also considered to be amyloid. Instead of having the conformation of what is called the native folded protein, which is liable to become denatured<sup>14</sup>, amyloid proteins occur in a form that is impervious to denaturants. It is widely considered to exist as parallel in-register  $\beta$ -sheet<sup>15-17</sup>, although structures with antiparallel  $\beta$ -sheet have also been characterized<sup>18-21</sup>. Parallel  $\alpha$ -sheet has also been suggested as the structure adopted initially during amyloid formation<sup>22-27</sup>.  $\beta$ -sheets formed by amyloid proteins are widely considered to gain their exceptional stability by folding into helical nanotube structures<sup>28-40</sup> of varying dimensions. Many amyloid fibrils have been shown to have a cross- $\beta$  structure; that is the  $\beta$ -strands run perpendicular to the fibril axis. Although the cross- $\beta$  structure appears to be the dominant form of the amyloid protofilament, there is a great deal of conformational diversity in amyloid fibrils<sup>41</sup> and  $\beta$ -helix models have also been proposed<sup>42</sup>. This suggests that in some cases an amyloid protofilament may adopt a multi-strand helix structure and that the theory developed here can be applied.

Biophysical work on several amyloid proteins has provided some structural parameters without complete atomic level detail. We show how such information can be used to yield accurate models. These models suggest a new structure which we call the “ $\beta$ -strip helix”, a set of in-register  $\beta$ -strands that become folded into a helix with strands that run nearly perpendicular to the fibril axis. The predicted helical nanotubes exhibit a register shift, both at the edges of single strips and at the join between adjacent  $\beta$ -strip helices. The register shift is a parameter of particular interest because its relationship to repeat sequences, the existence of which may help stabilise these structures.

## METHODS

The shear number was introduced by McLachlan<sup>7</sup> and elaborated upon later by Murzin et al.<sup>8</sup>. It is defined for  $\beta$ -barrels of circular cross-section as follows. Select a strand and a particular residue,  $k$ , on this strand. Step around the barrel from one strand to the next via residues aligned by hydrogen bonding (in a direction perpendicular to the strand direction) until the selected strand is reached again at residue  $l$ . The shear number,  $s$ , is defined as  $s=|l-k|$ . Here we take this concept further for homo-oligomeric multi-strand helices. To this end we introduce the “ $\beta$ -strip”.

### **$\beta$ -strip as repeating unit**

We define a  $\beta$ -strip as comprising  $m$  neighbouring  $\beta$ -strands (parallel, antiparallel or mixed) that constitute the minimal unit from which the whole multi-strand helix can be constructed via the symmetry operations of the  $n$ -fold rotational axis,  $C_n$ , which is also the helical axis. In most cases each strip corresponds to one single subunit in a homomeric molecule, however, as we shall see for  $\gamma$ -haemolysin, a strip can comprise strands from different, non-identical, subunits. With  $n$  strips, each comprising  $m$  strands, the total number of strands is  $nm$ . Fig 1 shows schematics of the unfolded 2D form and the native folded 3D form of a multi-strand helix comprising 3-stranded  $\beta$ -strips. The approach of using the unfolded 2D representation has been employed by Tsai et al. in a general method for the design of helical nanotubes comprising protein building blocks<sup>43</sup>.

### **Register-shift between $\beta$ -strips**

If in a multi-strand helix residue  $k$  in strand  $j$  is aligned with residue  $l$  in strand  $j+m$ , the corresponding strand in a neighbouring strip, then the register shift is  $t=|l-k|$ . For  $n$  strips the shear number is given by  $s=nt$  (Fig 1), the sum around the helix of the fixed register shift between neighbouring  $\beta$ -strips. Another way to think of the shear number is as a register-shift

of a strip with itself, i.e. a self register shift. The register shift,  $t$ , is even because consecutive main-chain CO and NH groups along the strand point in opposite directions.

### Equations relating $n$ , $m$ and $t$ to helical dimensions of the multi-strand helix

From the 2D depiction of Fig 1 the following holds for a multi-strand helix of *any* cross-sectional shape:

$$\tan(\alpha) = \frac{a_c t}{b_c m} \quad [1a]$$

$$p^2 = (nta_c)^2 + (nmb_c)^2 \quad [1b]$$

where  $t/m$  gives the register-shift between neighbouring strips per strand of the  $\beta$ -strip,  $\alpha$  is the angle between helical axis and strand direction,  $p$  is the length of the cross-sectional perimeter, and  $a_c$  and  $b_c$  are defined by two types of helices that exist within such a structure.

The “strand helix” is the helix passing through the  $C^\alpha$  atoms on any single strand. The “neighbour helix” is the helix passing through  $C^\alpha$  atoms of aligned residues which crosses the strand helix at right angles.  $a_c$  is the distance along the helical arc of the strand helix between consecutive  $C^\alpha$  atoms and  $b_c$  is the distance along the helical arc of the neighbour helix between consecutive  $C^\alpha$  atoms. From Fig 1 it can also be seen that the number of residues per turn,  $N_T$ , is given by  $N_T = (p^2 + h^2)^{1/2} / a_c$ .

Eq.1b corresponds to the “symmetrical” equation given by Murzin et al.<sup>8</sup>. However, both Murzin et al. and McLachlan used equations developed specifically for  $\beta$ -barrels which we show in Supplementary Method (Method.S1) become increasingly inaccurate the greater the

angle between the strand direction and the helical axis, and break down completely for a single-stranded  $\beta$ -helix. Eq. 1a and Eq. 1b, however, are exact even for a single-stranded  $\beta$ -helix. The approximation required to use them involves substituting the helical arc distances  $a_c$  and  $b_c$  by their helical chord equivalents  $a$  and  $b$ , which are presumed to be invariants determined by structural constraints. In the Supplementary Method we show that this is a very good approximation for all realizable  $\beta$ -helices and  $\beta$ -barrels of circular cross-section and all equations below will contain  $a$  and  $b$  rather than  $a_c$  and  $b_c$ . Furthermore, we put  $p=cd$ , where  $d$ , is the “width” of the helix as the perimeter is always proportional to a characteristic length if the shape is simply scaled without distortion. As we want to make a connection with the width measured by experimental techniques such as X-ray fibre diffraction then  $d$  so defined must span across the whole cross-section, so a reasonable definition would be the length of the longest characteristic “side”. If it has circular cross-section,  $d$  would be the diameter and  $c=\pi$ ; if it has triangular cross-section triangle, and  $d$  is the length of the longest side then one can show via the triangle inequality that in general  $2 < c \leq 3$ , and  $c=3$  when an equilateral triangle. A value of  $c=2$  cannot realistically occur as it implies a one-dimensional structure. For any irregular quadrilateral one can also show again using the triangle inequality that  $2 < c < 4$ . Some  $\beta$ -helices have “L”-like shapes (e.g. the HET-s(218-289) prion, see below) and it is trivial to show that for all “L”s, even those that have differing thicknesses and lengths of the horizontal and vertical arms,  $2 < c < 4$ . Larger values for  $c$  would only occur for more complex spikey shapes, but these do not occur in  $\beta$ -helices and  $\beta$ -barrels. Therefore we can state with reasonable confidence that  $2 < c < 4$ , when  $d$  is the length of the longest “side”. It is important to bear in mind that different shapes can have the same value of  $c$ .

The height per turn or pitch,  $h$ , can be seen in Fig 1 to relate to  $\alpha$  and  $p$  through,  $\tan(\alpha) = p/h = cd/h$ . Substituting into Eq. 1a and Eq. 1b gives, respectively:

$$\frac{t}{m} = \frac{b}{a} \frac{cd}{h} \quad [2a]$$

$$nm = \frac{cdh}{b\sqrt{(cd)^2 + h^2}} \quad [2b]$$

where  $nm$  is the number of strands in the helix. If  $m$  is known, Eq.2a and Eq.2b give the register shift and the number of strips, from helical dimensions  $d$  and  $h$ . It is also useful to be able to determine the helical dimensions from the number of strands and the register shift.

They are given by:

$$d = \frac{bnm}{c} \sqrt{\left(\frac{a}{b} \frac{t}{m}\right)^2 + 1} \quad [3a]$$

$$h = bnm \sqrt{\left(\frac{1}{\frac{a}{b} \frac{t}{m}}\right)^2 + 1} \quad [3b]$$

Solving Eq.3a and Eq.3b for  $t/m$  gives:

$$\frac{t}{m} = \frac{b}{a} \sqrt{\left(\frac{cd}{bnm}\right)^2 - 1} \quad [4a]$$

$$\frac{t}{m} = \frac{b}{a} \frac{1}{\sqrt{\left(\frac{h}{bnm}\right)^2 - 1}} \quad [4b]$$

Eq.4a and Eq.4b give lines of constant  $d$  and  $h$  in the  $(nm, t/m)$  plane, which means that, if the values of only two of these four are known, the plots can be used to determine the values of the remaining two.  $nm$  gives the total number of strands in the  $\beta$ -barrel or  $\beta$ -helix, while  $t/m$  gives the register-shift between neighbouring strips, per strand of the  $\beta$ -strip.

The expressions within the square root in Eq.4 give limiting conditions on  $nm$  for two extreme structures. Eq.4a gives the limiting condition  $nm=cd/b$ , which occurs when the strands are parallel with the helical axis and  $h$  is infinite. For a given cross-sectional width, it gives an upper limit on the number of strands. Structures in this region are  $\beta$ -barrel-like and the shear number  $s$  has low values. Eq.4b gives the limiting condition  $nm=h/b$ , which occurs when the strands are perpendicular to the helical axis, i.e. they are in the cross- $\beta$  configuration. For a given height per turn it gives an upper limit on the number of strands. Structures in this region are  $\beta$ -helix-like and  $s \approx cd/a$ , i.e. the shear number is approximately equal to the number of residues per turn.

### Mass-per-length of a multi-strand helix

The mass-per-length (MPL) of a fibril is a quantity that can be measured by electron microscopy (EM) techniques. Within the multi-strand helix model the following expression can be derived for the MPL,  $m_{PL}$ :

$$m_{PL} = \frac{nM_s}{La \cos(\alpha)} \quad (5)$$

where  $M_s$  is the molecular mass of the strip and  $L$  is the length of the strip in number of residues. From Fig 1 one can see that  $p\cos(\alpha)=nmb$  which substituted into Eq.5 gives:

$$p = \frac{ab}{\left(\frac{M_s}{mL}\right)} m_{PL} = \frac{ab}{m_{aa}} m_{PL} \quad (6)$$

where  $m_{aa}$  is the molecular mass of the strip per residue of the strip, which if unknown can be approximated by the average molecular mass of an amino acid residue. Given that  $p=cd$ , we find that, for a given cross-sectional shape, the width of the multi-strand helix is directly proportional to the MPL:

$$d = \frac{ab}{cm_{aa}} m_{PL} \quad (7)$$

Thus measurement of the MPL can be used to determine the width in all such multi-strand helices.

An expression that relates  $t/m$  to  $nm$  given the MPL is:

$$\frac{t}{m} = \frac{b}{a} \sqrt{\left(\frac{am_{PL}}{m_{aa}nm}\right)^2 - 1} \quad (8)$$

As a lot of new terms have been introduced, Table 1 gives a convenient summary of their definitions.

Although the expressions above have been derived in the context of homomeric structures with  $n$ -fold rotational symmetry, all are valid for those cases where  $n=1$  (formally 1-fold

symmetry) and as such can be applied to classic single-stranded  $\beta$ -helices,  $\beta$ -helices comprising a single  $\beta$ -strip forming a helical structure, or conventional  $\beta$ -barrels within in a single subunit or monomer.

## RESULTS

The distances  $a$  and  $b$  and were set to 3.3 Å and 4.8 Å, respectively. This value for  $a$  is the same used by Murzin et al.<sup>8</sup>, but they used a value of 4.4 Å for  $b$ , whereas McLachlan<sup>7</sup> used 4.72 Å, the former being clearly too short. We have used a value of 4.8 Å as this is often quoted in articles that report results from X-ray fibre diffraction experiments on amyloid fibrils as being the distance between strands in the cross- $\beta$  configuration. We set  $c=\pi$ . Unless experimental measurements suggest otherwise we will keep these values for  $a$ ,  $b$  and  $c$ . Eq.4a and Eq.4b were used to create a plot in the  $(nm, t/m)$  plane, shown in Fig 2, giving the range of possible multi-strand helices of circular cross-section, that is for  $c=\pi$ . Contour lines indicate the  $d$  and  $h$  values for each helix. As the angle  $\alpha$  is directly related to  $t/m$  it is indicated by the axis on the right of Fig 2. The shear number is given by  $s=nt=nm\times t/m$ , the area in the plot of the rectangle bounded by the axes and the vertical and horizontal lines passing through the point  $(nm, t/m)$ . Fig 3 shows contour lines in the  $(nm, t/m)$  plane for values of constant MPL created using Eq.8.

Measures of  $d$ ,  $h$ ,  $\alpha$ ,  $m$ ,  $n$  and  $t$ , referred to as having been determined directly from structures themselves, are either quoted from the literature or estimated from the deposited Protein Data Bank (PDB) files using the molecular graphics software, Pymol ([www.pymol.org](http://www.pymol.org)). As we have analysed regular structures they can be estimated with reasonable accuracy.

### Application to proteins of known structure

Two types of domain made from  $\beta$ -sheet in the form of a helical cylinder can be distinguished in native proteins:  $\beta$ -helices and  $\beta$ -barrels. In Fig 2A  $\beta$ -helices lie at the top left and have  $\alpha$  angles greater than  $75^\circ$  with the number of strands ( $nm$ ) 1, 2 or 3, while  $\beta$ -barrels are at the lower right and have  $\alpha$  angles not far from  $45^\circ$  with between 6 and 36 strands. Fig 2B focuses on  $\beta$ -helices while Fig 2C shows  $\beta$ -barrels. It is notable that none of the structures in Fig 2, mostly from native proteins, have  $t/m$  values less than 0.5.  $\beta$ -helices can be left-handed as well as right-handed but  $\beta$ -barrels in proteins, unlike  $\beta$ -helices, are always right-handed, not left-handed. Table 2 gives the key parameters for a representative selection of monomeric and homomeric multi-strand helices in native proteins.

Consideration of Fig 2 and Table 2 indicates three aspects of the distribution of the observed curved  $\beta$ -sheet helical structures in proteins worth emphasizing because of apparent anomalies compared to what is theoretically possible. Firstly the lack of left-handed  $\beta$ -barrels already mentioned is related to the propensity of strands of  $\beta$ -sheet to twist to the right looking along one strand<sup>44</sup>. Secondly the absence of  $\beta$ -barrels composed of strands parallel to the axis ( $t/m=0$ ,  $\alpha=0$ ), or of any with strands having  $t/m$  values less than 1 ( $\alpha < 19^\circ$ ), is also due to the tendency for strands to twist in one direction, though another factor is the side chain packing propensity for different types of barrels<sup>44</sup>. The third anomaly is the substantial gap between  $\beta$ -helices and  $\beta$ -barrels. In spite of the different nomenclature that has become established because in native proteins the two categories do not overlap, it is unclear why folded proteins so far analysed avoid this area of structure.

#### Homomeric $\beta$ -barrels

Examples of the various types of  $\beta$ -barrels in proteins are listed in Table 2. The commonest and best-known ones (filled  $\beta$ -barrels, hollow  $\beta$ -barrels and  $\alpha/\beta$ -barrels) have  $n=1$  and  $m>1$ , meaning that the strands in such barrels, though exhibiting a degree of symmetry to form the barrel, are non-identical, usually because they are different parts of a single subunit. Typical  $\beta$ -barrels are antiparallel while  $\alpha/\beta$ -barrels are parallel. When barrels are homomeric (formed from identical subunits) the possibility arises of true symmetry between strands so that  $n>1$  and  $m\geq 1$ ; such barrels are addressed below.

A group of related bacterial octameric or heptameric proteins involved in cell penetration and pore formation occur as antiparallel barrels with 14 or 16 strands. Two from *Staphylococcus* are described here. The transmembrane domain from the heptameric  $\alpha$ -haemolysin incorporates seven  $\beta$ -hairpins with 7-fold rotational symmetry ( $m=2$ ,  $n=7$ ,  $nm=14$ ), forming a 14-stranded antiparallel  $\beta$ -barrel<sup>45</sup> with circular cross-section as shown in Fig 4. The register shift,  $t=2$ , is measured between equivalent strands from neighbouring  $\beta$ -hairpins implying  $t/m=1$  to give  $\alpha=34.5^\circ$ . Eq.3 or Fig 2 give diameter  $d=26 \text{ \AA}$  and height per turn  $h=119 \text{ \AA}$ , which compare well with a diameter of  $26 \text{ \AA}$  and a height per turn in the range  $115\text{-}120 \text{ \AA}$ , estimated from the structure. The trans-membrane  $\beta$ -barrel pore of  $\gamma$ -hemolysin<sup>46</sup> has a circular cross-section and is an octamer with two similar but not identical types of subunit, each contributing a  $\beta$ -hairpin. It therefore has 4-fold rotational symmetry ( $m=4$ ,  $n=4$ ,  $nm=16$ ). The four  $\beta$ -strips each comprise four antiparallel  $\beta$ -strands, with a register-shift of four. Hence  $t/m=1$  and  $\alpha=34.5^\circ$ , which is similar to the measured value from the structure of  $35^\circ$ . Use of Eq.3 or Fig 2 leads to a height per turn is  $135 \text{ \AA}$  and a diameter of  $29.6 \text{ \AA}$ , which compares well with the measured diameter of  $30 \text{ \AA}$ .

The Mycobacterial outer membrane channel MspA is an octameric porin protein<sup>47</sup> from *M smegmatis*. It has a 16-stranded antiparallel  $\beta$ -barrel with a circular cross-section. It has 8-fold rotational symmetry being formed from eight  $\beta$ -strips, each comprising a  $\beta$ -hairpin, with a register shift of four. Here  $t/m=2.0$  and  $\alpha=54^\circ$ , which compares well with the observed value of  $56^\circ$ . This protein is shaped like a goblet, with one helical barrel, just described, forming the bulk of the stem. Below is a smaller, coaxial, helical barrel with a narrower diameter that can be regarded as the narrowed base of the goblet stem. The parameters of this smaller barrel are given in Table 2 and it is evident that it has a smaller  $t/m$  value of 1.0, giving rise to the lower angle  $\alpha$  and diameter  $d$ .

*E coli* TolC is one member of a family of trimeric efflux proteins in the outer membrane of gram-negative bacteria that are part of the type I secretion system. It has 3-fold symmetry, each  $\beta$ -strip comprising four antiparallel strands to give a 12-stranded antiparallel  $\beta$ -barrel<sup>48</sup>. The register shift is 8 giving  $t/m=2.0$ . *H influenzae* adhesin Hia is an autotransporter protein component of the bacterial type Vc secretion system<sup>49</sup>; it belongs to another family of trimeric proteins in which three four-stranded  $\beta$ -strips assemble to a 12-stranded antiparallel  $\beta$ -barrel<sup>50</sup> that anchors it to the outer membrane. Compared with TolC, a difference is that  $t/m=1.0$  such that the barrels are longer and thinner.

Several homomeric examples of  $\beta$ -barrels are not hollow, and do not normally occur in membranes. Fig 5 shows cylindrin, a toxic small amyloid-forming oligomer<sup>35</sup>, which has been suggested<sup>19,51</sup> as the material of the amyloid intermediate that is damaging to cells. It comprises three  $\beta$ -hairpins to form a 6-stranded antiparallel  $\beta$ -barrel of circular cross-section. Although not strictly homomeric and lacking perfect symmetry, the presence of a tandem repeat means that it can be regarded as such if the turn regions are ignored. The register shift

measured between equivalent strands from neighbouring  $\beta$ -hairpins from the N-terminal and the C-terminal repeat-sequences is 2. Therefore in this case  $t/m=1$ , giving  $\alpha=34.5^\circ$ , matching the measured value of  $35^\circ$ <sup>35</sup>. Using Eq.3 or Fig 2 gives a diameter  $d=11.2 \text{ \AA}$ , which compares well with the measured diameter of  $11 \text{ \AA}$ .

Muconolactone isomerase is one example of a family of dimeric " $\alpha+\beta$  barrels" that all incorporate a 2-fold symmetric, 8-stranded  $\beta$ -barrel, half from each subunit, with  $t/m=1.5$ .

The C-terminal domains of the four small subunits of the red-like form of RUBISCO (ribulose 1,5-bisphosphate carboxylase/oxygenase) associate to form a 4-fold symmetric 8-stranded antiparallel  $\beta$ -barrel with  $t/m=1.0$ . GTP cyclohydrolase is a pentameric enzyme; each subunit contributes four strands of a 20-stranded 5-fold symmetric  $\beta$ -barrel, for which  $t/m=1.0$ .

The structure crystal structure of CsgG, a lipoprotein that forms a secretion channel for curli subunits has been solved<sup>52</sup>. The transmembrane  $\beta$ -barrel is a nonamer with 9-fold symmetry where each subunit is a 4-stranded antiparallel  $\beta$ -strip. The register shift between neighbouring strips is 2 which means that  $t/m=0.5$ . This would give  $\alpha=19.0^\circ$  which means the strands are more aligned with the helical axis compared to other examples (see Fig2C) and is very much an outlier amongst  $\beta$ -barrels. Using Eq.3 we find  $d=58.2 \text{ \AA}$  which corresponds to the measured value from the structure directly of  $59 \text{ \AA}$ .

It is noticeable that the homomeric  $\beta$ -barrels frequently have  $\alpha=34.5^\circ$  corresponding to  $t/m=1.0$ .

*$\beta$ -helices*

Examples of right-handed  $\beta$ -helices in proteins are listed in Table 2. Single-strand  $\beta$ -helices, which are all parallel, are by far the commonest. Two-strand ones are antiparallel. The triple-strand  $\beta$ -helices<sup>53</sup> are trimeric and parallel.

A family of related proteins assemble into 3-start triple-strand  $\beta$ -helices<sup>54,55</sup>; those in the outer membranes of bacteria are part of the type VI secretion system, while those in phage belong to the bacterial cell penetration mechanism (homologous to the type VI secretion system). Fig 6 shows the non-contracted form of the tail spike from the T4 phage which has an approximate 3-fold rotational symmetry with  $t/m=8$ , giving by Eq. 1a,  $\alpha=79.7^\circ$ . Having a cross section that approximates an equilateral triangle quite well we put  $c=3$ , and using Eq. 3 we find that  $d=26.8 \text{ \AA}$  and  $h=14.6 \text{ \AA}$ . These values correspond well to those estimated from the structure itself: the length of the side of the triangle is approximately  $25 \text{ \AA}$  and the height per turn,  $15 \text{ \AA}$ . Although Fig 2B is with  $c=\pi$ , it can be plotted with reasonable accuracy on this figure.

The T4 spike is the central part of the phage tail. In addition two types of fibre, long and short, protrude from the centre of the tail. The structure of the short tail has been determined<sup>56</sup> and is also observed to be a trimer, part of which is also a triple-strand  $\beta$ -helix. This  $\beta$ -helix is somewhat shorter than the more central one, and  $t/m=6$ .

An endosialidase<sup>57</sup> from the tails of phage K1F that infects E coli also exhibits a short regular triple-strand  $\beta$ -helix with  $t/m=7$ .

Many examples of single-strand  $\beta$ -helices occur. Their cross-sectional shapes can be oval, square, triangular or L-shaped. They are fairly regular, and sometimes quite long, such that

estimates of shear values are worthwhile. Both left-handed and right-handed  $\beta$ -helices occur frequently but only right-handed ones are included in Fig 2 and Table 2 (although the theory developed is equally applicable to left-handed helices). One example is pectin lyase for which  $s=t/m=23$ . Another is given by the pentapeptide repeat proteins; they are square in cross-section, and have  $s=t/m=20$ .

### Amyloid Fibrils

It has been proposed that amyloid proteins are  $\beta$ -helix-like<sup>58</sup>. We present two atomic resolution structures that conform to the multi-strand helix model presented here. Details are given in Figs 2 and 7 and in Table 2.

### *HET-s(218-289) fibril*

The atomic resolution structure of HET-s(218-289) infectious form of the prion protein from *Podospora anserina* determined by solid state NMR<sup>2,59</sup> is a  $\beta$ -solenoid or more precisely a  $\beta$ -helix formed from four  $\beta$ -strands that form nearly two turns as shown in Fig 7A. Its cross-section has an approximate “L” shape. The register-shift is 36, which with  $n=1$  and  $m=1$ , gives  $d=37.8$  Å and  $h=4.8$  Å, which correspond well with the values estimated from the structure ( $d=38-40$  Å and  $h=4.8$  Å). The 36 residue register shift in HET-s(218-289) brings two 21-residue pseudo repeat sequences 15 residues apart into register. This repeat stabilises the  $\beta$ -helix itself and the joins between individual strands (subunits) in the fibril. This is depicted in Fig 7A and is considered further in the Discussion section.

### *Alzheimer A $\beta$ (40) NMR structure*

A solid-state NMR structure of the Alzheimer A $\beta$ (40) protein<sup>60</sup> also conforms to this model. It has three-fold symmetry about the fibril axis with a triangular cross-section. Each side of

the prism is formed by two  $\beta$ -sheet layers as shown in Fig 7B. The whole structure is built from chains aligned in register. The two  $\beta$ -sheet layers form a rectangle in cross-section (it is a  $\beta$  sandwich) and, although the  $\beta$ -strands are referred to as being in the cross- $\beta$  configuration, they are sufficiently at an angle to the fibril axis that Val40 in chain A joins with His13 in chain D giving rise to a continuous  $\beta$ -helical like arrangement when considering the mainchain paths (see Fig 7B). Residue 13 in chain D could be regarded as the first residue in the continuation of chain A which would be residue 41. In other words residue  $i$  in chain  $j+3$  can be regarded as residue number " $i+28$ " in its continuation of chain  $j$ . The register shift is therefore 28 as residues  $i$  in chain  $j$  are aligned through  $\beta$ -sheet hydrogen bonding with residues " $i+28$ " in chain  $j+3$ . Thus three in-register strands form a  $\beta$ -strip with  $n=1$ ,  $m=3$ , and  $t=28$ . We have called a helical structure formed from a single  $\beta$ -strip of in-register strands, a " $\beta$ -strip helix", and this is another example, albeit not an ideal one. With  $n=1$ ,  $m=3$ , and  $t=28$  the position of the structure in Fig 2B shows that it is not far from the T4 phage spike structure. With  $t/m=9.3$  and  $n=1$  we find  $d=29.8$  Å and  $h=14.3$ . Although the structure is irregular at the termini and turns we can estimate the cross-section to have a width along the longest side of about 32-37 Å and the height per turn to be approximately 15 Å. We find that  $\alpha=81.3^\circ$  indicating that the strands are, on average, only about  $9^\circ$  off the perfect cross- $\beta$  configuration and  $N_T=28.6$ , meaning that the structured part of each chain makes nearly one full turn in a  $\beta$ -helix-like conformation. In contrast to the HET-s structure, where two separate but similar sequence segments stabilise both the  $\beta$ -strip helix structure and joining of the subunits, here all 28 residues from His13 to Val40 in each  $\beta$ -strip helix can join end-to-end and in register to create the growing protofilament.

### Modelling amyloid protofilaments from limited experimental data

Using proteins of known structure we have shown that the method accurately predicts  $d$  and  $h$  (or  $\alpha$ ) from  $t/m$  and  $nm$ . With amyloid it is often not possible to determine an atomic resolution structure. In X-ray fibre diffraction experiments equatorial reflections relate to the width of the fibril,  $d$ , and meridional reflections relate to a repeat along the fibril axis, possibly giving  $h$ . Sometimes the angle  $\alpha$  can also be determined. Other methods such as small angle X-ray (SAXS) and neutron (SANS) scattering<sup>61</sup> which do not rely on fibril orientation, can also be used to determine fibril dimensions. EM techniques can be used to determine the MPL and spectroscopic methods such as NMR and electron paramagnetic resonance (EPR) can be used to determine register-shifts, possibly giving values for  $t$ . Protein stoichiometry methods could also determine  $n$ . Experimental measurements give fibril dimensions, whereas the proposed multi-strand helix is a model for the constituent protofilament. However any two of the following six quantities  $nm$ ,  $t/m$ ,  $d$ ,  $h$ ,  $\alpha$  and  $m_{PL}$  that relate to the protofilament have been experimentally determined, the values for the remaining can be determined (this applies to all 15 pairs apart from  $d$ ,  $m_{PL}$ , and  $\alpha$ ,  $t/m$ ).

If  $nm$  and  $t/m$  are estimated from experimental values of  $d$  and  $h$  using Eq. 1a and Eqs.2, we first round off  $nm$  to the nearest integer and then adjust  $t/m$  so that  $s = nm \times t/m$  is equal to the nearest even integer, given that  $s$  must be even. Below we take this approach to create backbone models for transthyretin and Alzheimer A $\beta$ (40) from X-ray fibre diffraction experiments. In Supplementary Result (Result.S1) we show how knowledge of the MPL of the HET-s(218-289) prion from EM,<sup>62</sup> and the residue number distance between the repeat sequences, can be used to predict the helical structure.

*Transthyretin model from X-ray fibre diffraction measurements*

X-ray fibre diffraction of transthyretin amyloid fibril indicates a protofilament with  $d_{exp}=30$  Å and a repeating unit along the protofilament axis (meridional reflection) of 115.5 Å with the strands arranged in cross- $\beta$  configuration<sup>63</sup>. For a distance of 4.8 Å between strands, this suggests a repeating unit comprising 24 strands<sup>63</sup>. From Fig 2 a multi-strand helix with  $d=30$  Å and  $nm=24$  is impossible. Meridional reflections also suggest an axial repeat distance of 29 Å, which we take as the value of  $h_{exp}$ . We consider two models, one cylinder with  $c=\pi$ , and one triangular prism, with  $c=3$ . The position of the cylinder is plotted on Fig 2B and results of the analysis for both models are given in Table 3. For both  $nm_{mod}=6$  and  $t/m_{mod}=4.67$ . As  $n$ ,  $m$  are integers and  $t$  an even integer, and assuming that proteins are formed from in-register  $\beta$ -sheet<sup>15,17</sup>, an appropriate choice is  $n_{mod}=1$ ,  $m_{mod}=6$  and  $t_{mod}=28$ , that is, it is a  $\beta$ -strip helix formed from six strands. With  $N_{T_{mod}}=31$  residues and 127 residues in the transthyretin subunit, the multi-strand-helix has 4.1 turns. Both models have a length of 115.6 Å (measured across four turns), matching the repeat distance of 115.5 Å from X-ray fibre diffraction. This suggests that like the HET-s and the Alzheimer A $\beta$ (40) NMR structures, the  $\beta$ -strip helices, each a protofilament subunit, join end-to-end with  $\beta$ -sheet hydrogen bonding to form the protofilament. Thus the 115.5 Å repeat could be due to the regularly spaced joins between protofilament subunits and the 29 Å repeat due to a helical seam in the  $\beta$ -strip helix running along the join between the opposite sides of the  $\beta$ -strip where the sequences are out-of-register. Fig 8A depicts the cylinder model protofilament subunit and two protofilament subunits joined end-to-end. This paper model can be created using Supplementary Figure, Fig.S1.

#### Alzheimer A $\beta$ (40) model from X-ray fibre diffraction measurements

Fraser et al<sup>64</sup> reported X-ray fibre diffraction work on Alzheimer A $\beta$ (40) fibres that gave  $d_{exp}=28$  Å and  $\alpha_{exp}=54.4^\circ$  for the protofilament<sup>64-66</sup>. This is an atypical structure as it does

not have the usual cross- $\beta$  arrangement but is illustrative in showing how to create a backbone model knowing  $d_{exp}$  and  $\alpha_{exp}$  only. The position of the structure with circular cross-section ( $d_{exp}=28 \text{ \AA}$ ,  $\alpha_{exp}=54.4^\circ$ ) is plotted on Fig 2C. The measured distance between strands in these experiments is  $4.7 \text{ \AA}$ , so we use this value for  $b$  instead of  $4.8 \text{ \AA}$ . The results are given in Table 3. For both cylinder and prism models  $t/m_{mod}=2$ , but the prism has  $nm_{mod}=10$  whereas for the cylinder  $nm_{mod}=11$ . Site-directed spin labelling experiments on A $\beta$ (40) amyloid have shown that the strands are parallel and in register<sup>67</sup> implying a  $\beta$ -strip helix with 10 or 11 strands. For the prism model  $N_{Tmod}=30$  residues, it has 1.3 turns, and for cylinder model  $N_{Tmod}=33$ , it has 1.2 turns. Measured across one turn, the lengths are  $51.9 \text{ \AA}$  for the prism and  $57.7 \text{ \AA}$  for the cylinder. These predicted distances are close to the axial repeat distance of  $57 \text{ \AA}$  found in the same fibre diffraction experiment<sup>64</sup>. Other axial repeat distances reported are  $53 \text{ \AA}$ <sup>68</sup> and  $54 \text{ \AA}$ <sup>69</sup>. Again this suggests that  $\beta$ -strip helices, each a protofilament subunit, join end-to-end with  $\beta$ -sheet hydrogen bonding to form the protofilament and that the  $57 \text{ \AA}$  repeat is due to the join between subunits. Fig 8B shows a depiction of the prism model protofilament subunit and two protofilament subunits joined end-to-end. Folded paper models of these structures can be created using Supplementary Figures, Fig.S2, and Fig.S3.

With a molecular mass of 4.33 kDa for a single A $\beta$ (40) molecule, the 10-stranded and 11-stranded models have MPLs of  $\sim 5.6 \text{ kDa/nm}$  and  $\sim 6.2 \text{ kDa/nm}$ , respectively. Electron microscopy measurements suggest a protofilament with an MPL of  $\sim 9 \text{ kDa/nm}$ <sup>70</sup>, which, keeping  $t/m=2$ , suggests a structure with  $m=16$ . Such a structure, with the same value for  $c$ , is wider than those based on the X-ray diffraction results alone.

## DISCUSSION

We present equations for the geometrical relationships of helical nanotubes with multiple subunits, applying to both  $\beta$ -barrels and  $\beta$ -helices. Previous equations<sup>5,6</sup> did not cater for homo-oligomeric proteins and were applicable to  $\beta$ -barrels only. The concept of a  $\beta$ -strip is introduced, defined as the minimal repeating unit within the multi-strand helix. The relationships between  $m$ , the number of strands in each strip,  $t$ , the register shift per strip,  $\alpha$ , the angle between the helical axis and the strand direction,  $d$ , the width and  $h$ , the rise per turn are described.  $nm$  gives the total number of strands. The usefulness of the quantity  $t/m$ , which can be regarded as the register shift per strand of the strip, is stressed; it is directly related to the angle  $\alpha$ , measurable via X-ray fibre diffraction, through the equation  $t/m=1.45\tan(\alpha)$ .

We show that in a single graph of constant  $d$  and  $h$  in the  $(nm,t/m)$  or  $(nm,\alpha)$  plane, as in Fig 2, is useful for comparing and appreciating the diversity of structures of regular-shaped  $\beta$ -helices and  $\beta$ -barrels, whether forming multiple subunits or not. The plots reveal that, while there is no inherent difference between a  $\beta$ -helix and a  $\beta$ -barrel in that the ranges of possible structures merge into one another, those found in native proteins do occur in the two easily-defined groupings. A good discriminator is  $t/m$  (or  $\alpha$ ): for  $\beta$ -helices  $t/m$  is 6 or above ( $\alpha>76^\circ$ ) while for  $\beta$ -barrels  $t/m$  is between 0.5 and 2.5 ( $\alpha=19-60^\circ$ ). A feature seen in Fig 2C is that the majority of homomeric  $\beta$ -barrel structures have  $t/m=1$  and therefore  $\alpha=34.5^\circ$ .

We have shown that the MPL is directly proportional to the length of the cross-sectional perimeter and can be used to estimate the cross-sectional width. In the case of a fibril, this relationship may be used to estimate its width when only the MPL is available. Alternatively if both MPL and protofilament width are measurable, the same relationship can be used to test whether the structure conforms to the multi-strand helix model proposed here. A

convenient expression relating width and MPL derived from Eq.7 is

$d(\text{nm}) \approx 0.46 m_{PL}(\text{kDa}/\text{nm})$ , for a circular cross-section.

The equations developed can also be used to estimate the values of  $t/m$  and  $nm$  given knowledge about the helix dimensions such as  $d$  and  $h$ . In the case of the transthyretin amyloid protofilament it is intriguing that the predicted nanotube, based on dimensions from X-ray fibre diffraction, has  $t/m=4.5-4.7$  and  $nm=5.8$ , midway between a  $\beta$ -helix and a  $\beta$ -barrel. For the  $A\beta(40)$  amyloid model, the predicted nanotube is a somewhat more conventional barrel-like structure in terms of its values for  $t/m$  of 2.0 and  $nm$  of 10-11.

The predicted transthyretin and  $A\beta(40)$  amyloid structures could occur with  $n>1$ , incorporating more than one  $\beta$ -strip. For example, instead of  $n=1$ ,  $m=6$ ,  $t=28$  two  $\beta$ -strips,  $n=2$ ,  $m=3$ ,  $t=14$ , could assemble to a multi-strand helix. However, all such helices are situated in the same position on Fig 2 and once assembled are liable to be indistinguishable.

Some amyloid protofilament structures are thought to comprise structures with antiparallel strands<sup>19,20,51</sup>. The ideas presented here can accommodate structures with strands that are parallel, antiparallel or a mixture of the two, as this will depend on the structure of the  $\beta$ -strip. For example, a multi-strand helix with antiparallel strands can be formed through  $\beta$ -hairpins coming together with a fixed register shift.  $\alpha$ -haemolysin shown in Fig 4 provides an example.

The transthyretin and  $A\beta(40)$  helical structures are listed in Table 2 as having  $n=1$ , in spite of being homomeric assemblies, i.e. they are homomeric but do not have rotational symmetry.

This arrangement could lead to them being classified as  $\beta$ -helices. On the other hand their

general appearance, as in Fig 8, and their various helical dimensions, are more in keeping with  $\beta$ -barrels. A conclusion is that these are novel helical assemblies with properties of both types of structure. We call these structures “ $\beta$ -strip helices”. Their formation involves the association of polypeptides in-register to form a normal parallel  $\beta$ -sheet. As a  $\beta$ -sheet has a natural tendency to twist it curls round such that the main-chain atoms of the two outer strands hydrogen bond to one another with a register shift, as in Fig 8C.

The multi-strand helix is a possible model for an amyloid protofilament but amyloid fibrils comprise a number of intertwined protofilaments indicating a natural tendency for the protofilaments to twist. In this regard it is interesting to see that the comparatively long  $\beta$ -helix in the T4 phage spike has a natural twist. Although protofilaments may have inherent twist, or an ability to twist due to natural flexibility, the degree of twisting must be limited, as the quantities  $n$ ,  $m$ , and  $t$ , should not vary if structural integrity of the protofilament is to be maintained. Further studies may be able to determine the variety of fibrils that can be constructed from intertwining protofilaments with the same  $n$ ,  $m$ , and  $t$  values.

The A $\beta$ (40) amyloid protofilament model presented here is based on an X-ray fibre diffraction experiment that indicated the strands are tilted by  $\sim 35^\circ$  to the usual cross- $\beta$  configuration. This is at odds with more recent in-register atomic resolution structures determined by NMR methods that show the cross- $\beta$  structure<sup>60,71-74</sup>. Even so one of these structures conforms to the model with the strands of the  $\beta$ -strip helix running about  $9^\circ$  to the perfect cross- $\beta$  configuration. Although the solid state NMR structure presented by Petkova et.al.<sup>72</sup> did not have a  $\beta$ -helical form, the authors mention that their experimental data did not rule out the possibility that “the C-terminus of one A $\beta$ (40) chain would contact a residue near the N terminus of the next chain in the cross- $\beta$  unit.”

A feature of the HET-s amyloid is that within the same subunit the N-terminal repeat-sequence (residues 226-246) aligns with the C-terminal repeat-sequence (residues 262-282) to form the mainchain-mainchain hydrogen bonding of the  $\beta$ -helix as seen in Fig 7A. If we denote the N-terminal repeat sequence in chain A as “N<sub>A</sub>” and the C-terminal repeat sequence in chain A as “C<sub>A</sub>”, the same alignment is seen at the join of individual subunits: that is C<sub>A</sub> aligns with N<sub>B</sub> in chain B. The sequence of alignments could be denoted N<sub>A</sub>:C<sub>A</sub>|N<sub>B</sub>:C<sub>B</sub>|N<sub>C</sub>:C<sub>C</sub>.., where “:” denotes an alignment within a subunit and “|” a subunit join.

Thus the alignment of the N-terminal and C-terminal repeat-sequences stabilises the  $\beta$ -helix structure, both within individual subunits and at inter-subunit joins. An attractive feature of our A $\beta$ (40) model is that N-terminal residues 1-20 (in the case of the 10-stranded  $\beta$ -strip helix) align with C-terminal residues 21-40 within the  $\beta$ -strip helix, allowing the same residues on opposite sides of the strip to align via  $\beta$ -sheet hydrogen bonding to form inter-subunit joins in a process akin to that in the HET-s  $\beta$ -helix. An N-terminal-C-terminal repeat or pseudo repeat sequence is liable to facilitate this process in any in-register  $\beta$ -strip helix.

The idea that the distance between repeat sequences determines the register shift finds further support in the T4 phage spike structure, where REPPER<sup>75</sup>, a program that searches for repeat sequences, indicates a highly significant repeat of periodicity 8, matching the register shift seen in the structure.

We have developed the theory for the shear number for application to homomeric structures. The development leads naturally to the concept of the  $\beta$ -strip, the basic unit from which the whole helical structure can be generated giving it  $n$ -fold rotational symmetry. In this context the shear number can be interpreted in terms of the well-known concept of register shift. The shear number was developed in the context of a single-stranded  $\beta$ -barrel, whereas the theory

presented here is equally applicable to  $\beta$ -helices. In fact it is valid for all kinds of multi-strand helices, homomeric or non-homomeric, irrespective of their cross-sectional shape. Its accuracy and wide applicability has been demonstrated using a number of known atomic resolution structures and plotting these in the  $(nm, t/m)$  or  $(d, h)$  parameter space reveals that  $\beta$ -helix and  $\beta$ -barrel are at two ends of the same spectrum separated by an unoccupied region. A natural application of this method is modelling of amyloid protofilaments as these are sometimes thought to be built from  $\beta$ -helices. We have shown how measurement of helical dimensions from X-ray fibre diffraction of amyloid fibrils enables the prediction of other quantities of interest such as the register shift and the axial repeat distance. Models of protofilaments based on these findings suggest both stability of an individual protofilament subunit (a  $\beta$ -strip helix) and growth by association of protofilament subunits, involves the same sequence segments coming together with  $\beta$ -sheet hydrogen bonding at the same register shift. The results presented also have implications for the design of nanotubes as they demonstrate how the register shift, which relates to the dimensions of the helix, could be controlled by choosing a repeat sequence spaced accordingly.

## REFERENCES

1. Kajava AV, Steven AC.  $\beta$ -rolls,  $\beta$ -helices, and other  $\beta$ -solenoid proteins. *Adv Prot Chem* 2006;73:55-96.
2. Wasmer C, Lange A, Van Melckebeke H, Siemer AB, Riek R, Meier BH. Amyloid fibrils of the HET-s(218-289) prion form a  $\beta$  solenoid with a triangular hydrophobic core. *Science* 2008;319:1523-1526.

3. Mayans O, Scott M, Connerton I, Gravesen T, Benen J, Visser J, Pickersgill R, Jenkins J. Two crystal structures of pectin lyase A from *Aspergillus* reveal a pH driven conformational change and striking divergence in the substrate-binding clefts of pectin and pectate lyases. *Structure* 1997;5(5):677-689.
4. Banner DW, Bloomer AC, Petsko GA, Phillips DC, Wilson IA. Atomic coordinates for triose phosphate isomerase from chicken muscle. *Biochem Biophys Res Commun* 1976;72(1):146-155.
5. Galdiero S, Galdiero M, Pedone C.  $\beta$ -barrel membrane bacterial proteins: Structure, function, assembly and interaction with lipids. *Curr Protein Pept Sci* 2007;8:63-82.
6. Fairman JW, Noinaj N, Buchanan SK. The structural biology of  $\beta$ -barrel membrane proteins: a summary of recent reports. *Curr Opin Struct Biol* 2011;21:523-531.
7. McLachlan AD. Gene duplications in the structural evolution of chymotrypsin. *J Mol Biol* 1979;128:49-79.
8. Murzin AG, Lesk AM, Chothia C. Principles determining the structure of  $\beta$ -sheet barrels in proteins .1. A Theoretical-analysis. *J Mol Bio.* 1994;236:1369-1381.
9. Murzin AG, Brenner SE, Hubbard T, Chothia C. SCOP - A structural classification of proteins database for the investigation of sequences and structures. *J Mol Biol* 1995;247(4):536-540.

10. Sipe JD, Cohen AS. Review: History of the amyloid fibril. *J Struct Biol* 2000;130(2-3):88-98.
11. Buxbaum JN, Linke RP. A Molecular History of the Amyloidoses. *J Mol Biol* 2012;421:142-159.
12. Eisenberg D, Jucker M. The Amyloid State of Proteins in Human Diseases. *Cell* 2012;148:1188-1203.
13. Ritter C, Maddelein ML, Siemer AB, Luhrs T, Ernst M, Meier BH, et al. Correlation of structural elements and infectivity of the HET-s prion. *Nature* 2005;435:844-848.
14. de Groot NS, Sabate R, Ventura S. Amyloids in bacterial inclusion bodies. *Trends Biochem Sci* 2009;34:408-416.
15. Shewmaker F, McGlinchey RP, Wickner RB. Structural insights into functional and pathological amyloid. *J Biol Chem* 2011;286:16533-16540.
16. Shinchuk LM, Sharma D, Blondelle SE, Reixach N, Inouye H, Kirschner DA. Poly-(L-alanine) expansions form core  $\beta$ -sheets that nucleate amyloid assembly. *Proteins* 2005;61:579-589.
17. Wickner RB, Shewmaker F, Kryndushkin D, Edskes HK. Protein inheritance (prions) based on parallel in-register  $\beta$ -sheet amyloid structures. *Bioessays* 2008;30:955-964.

18. Lendel C, Bjerring M, Dubnovitsky A, Kelly RT, Filippov A, Antzutkin ON, et al. A Hexameric Peptide Barrel as Building Block of Amyloid- $\beta$  Protofibrils. *Angew Chem Int Ed Engl* 2014;53:12756-12760.
19. Rodriguez JA, Ivanova MI, Sawaya MR, Cascio D, Reyes FE, Shi D, et al. Structure of the toxic core of  $\alpha$ -synuclein from invisible crystals. *Nature* 2015;525:486-490.
20. Sawaya MR, Sambashivan S, Nelson R, Ivanova MI, Sievers SA, Apostol MI, et al. Atomic structures of amyloid cross- $\beta$  spines reveal varied steric zippers. *Nature* 2007;447:453-457.
21. Serra-Batiste M, Ninot-Pedrosa M, Bayoumi M, Gairi M, Maglia G, Carulla N. A $\beta$ 42 assembles into specific  $\beta$ -barrel pore-forming oligomers in membrane-mimicking environments. *Proc Natl Acad Sci U S A* 2016;113:10866-10871.
22. Armen RS, Alonso DOV, Daggett V. Anatomy of an amyloidogenic intermediate: Conversion of  $\beta$ -sheet to  $\alpha$ -sheet structure in transthyretin at acidic pH. *Structure* 2004;12:1847-1863.
23. Armen RS, DeMarco ML, Alonso DOV, Daggett V. Pauling and Corey's  $\alpha$ -pleated sheet structure may define the prefibrillar amyloidogenic intermediate in amyloid disease. *Proc Natl Acad Sci U S A* 2004;101:11622-11627.
24. Daggett V.  $\alpha$ -sheet: The toxic conformer in amyloid diseases? *Acc Chem Res* 2006;39:594-602.

25. Hayward S, Milner-White EJ. The geometry of  $\alpha$ -sheet: Implications for its possible function as amyloid precursor in proteins. *Proteins* 2008;71:415-425.
26. Hayward S, Milner-White EJ. Simulation of the  $\beta$ - to  $\alpha$ -sheet transition results in a twisted sheet for antiparallel and an  $\alpha$ -nanotube for parallel strands: Implications for amyloid formation. *Proteins* 2011;79:3193-207.
27. Milner-White EJ, Watson JD, Qi G, Hayward S. Amyloid formation may involve  $\alpha$ - to  $\beta$ -sheet interconversion via peptide plane flipping. *Structure* 2006;14:1369-1376.
28. Adams DJ, Holtzmann K, Schneider C, Butler MF. Self-assembly of surfactant-like peptides. *Langmuir* 2007;23:12729-12736.
29. Bucak S, Cenker C, Nasir I, Olsson U, Zackrisson M. Peptide Nanotube Nematic Phase. *Langmuir* 2009;25:4262-4265.
30. Castelletto V, Nutt DR, Hamley IW, Bucak S, Cenker C, Olsson U. Structure of single-wall peptide nanotubes: in situ flow aligning X-ray diffraction. *Chem Commun* 2010;46:6270-6272.
31. Childers WS, Mehta AK, Lu K, Lynn DG. Templating molecular arrays in amyloid's cross- $\beta$  grooves. *J Am Chem Soc* 2009;131:10165-10167.
32. Hamley IW. Peptide Nanotubes. *Angew Chem Int Ed* 2014;53:6866-6881.

33. Hamley IW, Dehsorkhi A, Castelletto V. Self-assembled arginine-coated peptide nanosheets in water. *Chem Commun* 2013;49:1850-1852.
34. Kaye R, Pensalfini A, Margol L, Sokolov Y, Sarsoza F, Head E, et al. Annular protofibrils are a structurally and functionally distinct type of amyloid oligomer. *J Biol Chem* 2009;284:4230-4237.
35. Laganowsky A, Liu C, Sawaya MR, Whitelegge JP, Park J, Zhao M, et al. Atomic view of a toxic amyloid small oligomer. *Science* 2012;335:1228-1231.
36. Lu K, Jacob J, Thiyagarajan P, Conticello VP, Lynn DG. Exploiting amyloid fibril lamination for nanotube self-assembly. *J Am Chem Soc* 2003;125:6391-6393.
37. Mehta AK, Lu K, Childers WS, Liang Y, Dublin SN, Dong J, et al. Facial symmetry in protein self-assembly. *J Am Chem Soc* 2008;130:9829-9835.
38. Morris KL, Zibae S, Chen L, Goedert M, Sikorski P, Serpell LC. The structure of cross- $\beta$  tapes and tubes formed by an octapeptide,  $\alpha$ S $\beta$ 1. *Angew Chem Int Ed* 2013;52:2279-2283.
39. Perutz MF, Finch JT, Berriman J, Lesk A. Amyloid fibers are water-filled nanotubes. *Proc Natl Acad Sci U S A* 2002;99:5591-5595.

40. Vauthey S, Santoso S, Gong HY, Watson N, Zhang SG. Molecular self-assembly of surfactant-like peptides to form nanotubes and nanovesicles. *Proc Natl Acad Sci U S A* 2002;99:5355-5360.
41. Toyama BH, Weissman JS. Amyloid Structure: Conformational Diversity and Consequences. In: Kornberg RD, Raetz CRH, Rothman JE, Thorner JW, editors. *Ann Rev Biochem* 2011;80:557-585.
42. Makin OS, Serpell LC. Structures for amyloid fibrils. *Febs J* 2005;272:5950-61.
43. Tsai CJ, Zheng J, Nussinov R. Designing a nanotube using naturally occurring protein building blocks. *PLoS Comput Biol* 2006;2:311-319.
44. Jang H, Arce FT, Ramachandran S, Capone R, Lal R, Nussinov R.  $\beta$ -barrel topology of alzheimer's  $\beta$ -amyloid ion channels. *J Mol Biol* 2010;404:917-934.
45. Song LZ, Hobaugh MR, Shustak C, Cheley S, Bayley H, Gouaux JE. Structure of staphylococcal  $\alpha$ -hemolysin, a heptameric transmembrane pore. *Science* 1996;274:1859-1866.
46. Yamashita K, Kawai Y, Tanaka Y, Hirano N, Kaneko J, Tomita N, et al. Crystal structure of the octameric pore of staphylococcal  $\gamma$ -hemolysin reveals the  $\beta$ -barrel pore formation mechanism by two components. *Proc Natl Acad Sci U S A* 2011;108:17314-17319.

47. Faller M, Niederweis M, Schulz GE. The structure of a mycobacterial outer-membrane channel. *Science* 2004;303:1189-1892.
48. Koronakis V, Sharff A, Koronakis E, Luisi B, Hughes C. Crystal structure of the bacterial membrane protein TolC central to multidrug efflux and protein export. *Nature* 2000;405:914-919.
49. Leo JC, Grin I, Linke D. Type V secretion: mechanism(s) of autotransport through the bacterial outer membrane. *Philos Trans R Soc B Biol Sci* 2012;367:1088-1101.
50. Meng G, Surana NK, St Geme JW, III, Waksman G. Structure of the outer membrane translocator domain of the *Haemophilus influenzae* Hia trimeric autotransporter. *EMBO J* 2006;25:2297-2304.
51. Do TD, LaPointe NE, Nelson R, Krotee P, Hayden EY, Ulrich B, et al. Amyloid  $\beta$ -Protein C-Terminal Fragments: Formation of Cylindrins and  $\beta$ -Barrels. *J Am Chem Soc* 2016;138:549-557.
52. Cao BH, Zhao Y, Kou YJ, Ni DC, Zhang XJC, et al. (2014) Structure of the nonameric bacterial amyloid secretion channel. *Proc Natl Acad Sci U S A* 111: E5439-E5444.
53. Mitraki A, Papanikolopoulou K, Van Raaij MJ. Natural triple  $\beta$ -stranded fibrous folds. *Adv Prot Chem* 2006;73:97-124.

54. Kanamaru S, Leiman PG, Kostyuchenko VA, Chipman PR, Mesyanzhinov VV, Arisaka F, et al. Structure of the cell-puncturing device of bacteriophage T4. *Nature* 2002;415:553-557.
55. Uchida K, Leiman PG, Arisaka F, Kanamaru S. Structure and properties of the C-terminal  $\beta$ -helical domain of VgrG protein from *Escherichia coli* O157. *J Biochem* 2014;155:173-182.
56. van Raaij MJ, Schoehn G, Burda MR, Miller S. Crystal structure of a heat and protease-stable part of the bacteriophage T4 short tail fibre. *J Mol Biol* 2001;314:1137-1146.
57. Stummeyer K, Dickmanns A, Muhlenhoff M, Gerardy-Schahn R, Ficner R. Crystal structure of the polysialic acid-degrading endosialidase of bacteriophage K1F. *Nat Struct Mol Biol* 2005;12:90-96.
58. Tsai HH, Gunasekaran K, Nussinov R. Sequence and structure analysis of parallel  $\beta$  helices: Implication for constructing amyloid structural models. *Structure* 2006;14:1059-1072.
59. Wasmer C, Schutz A, Loquet A, Buhtz C, Greenwald J, Riek R, et al. The Molecular Organization of the Fungal Prion HET-s in Its Amyloid Form. *J Mol Biol* 2009;394:119-127.
60. Paravastu AK, Leapman RD, Yau WM, Tycko R. Molecular structural basis for polymorphism in Alzheimer's  $\beta$ -amyloid fibrils. *Proc Natl Acad Sci U S A* 2008;105:18349-18354.

61. Avdeev MV, Aksenov VL, Gazova Z, Almasy L, Petrenko VI, Gojzewski H, Feoktystov AV, Siposova K, Antosova A, Timko M, Kopcansky P. On the determination of the helical structure parameters of amyloid protofilaments by small-angle neutron scattering and atomic force microscopy. *J Appl Crystallogr* 2013;46:224-233.
62. Sen A, Baxa U, Simon MN, Wall JS, Sabate R, et al. (2007) Mass analysis by scanning transmission electron microscopy and electron diffraction validate predictions of stacked beta-solenoid model of HET-s prion fibrils. *J Biol Chem* 282: 5545-5550.
63. Blake C, Serpell L. Synchrotron X-ray studies suggest that the core of the transthyretin amyloid fibril is a continuous  $\beta$ -sheet helix. *Structure* 1996;4:989-998.
64. Fraser PE, Nguyen JT, Inouye H, Surewicz WK, Selkoe DJ, Podlisny MB, et al. Fibril formation by primate, rodent, and Dutch-hemorrhagic analogs of Alzheimer amyloid  $\beta$ -protein. *Biochemistry* 1992;31:10716-10723.
65. Malinchik SB, Inouye H, Szumowski KE, Kirschner DA. Structural analysis of Alzheimer's  $\beta$ (1-40) amyloid: Protofilament assembly of tubular fibrils. *Biophys J* 1998;74:537-545.
66. Serpell LC. Alzheimer's amyloid fibrils: structure and assembly. *Biochim Biophys Acta* 2000;1502:16-30.

67. Torok M, Milton S, Kaye R, Wu P, McIntire T, Glabe CG, et al. Structural and dynamic features of Alzheimer's A  $\beta$  peptide in amyloid fibrils studied by site-directed spin labeling. *J Biol Chem* 2002;277:40810-40815.
68. Inouye H, Fraser PE, Kirschner DA. Structure of  $\beta$ -crystallite assemblies formed by Alzheimer  $\beta$ -amyloid protein analogs - Analysis by X-ray-diffraction. *Biophys J* 1993;64:502-519.
69. Fraser PE, Duffy LK, Omalley MB, Nguyen J, Inouye H, Kirschner DA. Morphology and antibody recognition of synthetic  $\beta$ -amyloid peptides. *J Neuro Res* 1991;28:474-485.
70. Chen B, Thurber KR, Shewmaker F, Wickner RB, Tycko R. Measurement of amyloid fibril mass-per-length by tilted-beam transmission electron microscopy. *Proc Natl Acad Sci U S A* 2009;106:14339-14344.
71. Luhrs T, Ritter C, Adrian M, Riek-Loher D, Bohrmann B, Doeli H, et al. 3D structure of Alzheimer's amyloid- $\beta$ (1-42) fibrils. *Proc Natl Acad Sci U S A* 2005;102:17342-17347.
72. Petkova AT, Ishii Y, Balbach JJ, Antzutkin ON, Leapman RD, Delaglio F, et al. A structural model for Alzheimer's  $\beta$ -amyloid fibrils based on experimental constraints from solid state NMR. *Proc Natl Acad Sci U S A* 2002;99:16742-16747.
73. Qiang W, Yau WM, Luo YQ, Mattson MP, Tycko R. Antiparallel  $\beta$ -sheet architecture in Iowa-mutant  $\beta$ -amyloid fibrils. *Proc Natl Acad Sci U S A* 2012;109:4443-4448.

74. Schutz AK, Vagt T, Huber M, Ovchinnikova OY, Cadalbert R, Wall J, et al. Atomic-resolution three-dimensional structure of amyloid  $\beta$  fibrils bearing the Osaka mutation.

Angew Chem Int Ed Engl 2015;54:331-335.

75 Gruber M, Soding J, Lupas AN. REPPER-repeats and their periodicities in fibrous proteins. Nucleic Acids Res 2005;33:W239-W243.

#### ACKNOWLEDGEMENTS

We thank Hanna Hayward for help in producing some of the figures.

## FIGURE LEGENDS

### Figure 1

#### Schematic showing geometry in 2D and 3D forms of a general multi-strand helix

Depiction of an unrolled/unfolded 2D form of a multi-strand helix of any general cross-sectional shape with perimeter length  $p$  and rolled-up cylinder form.  $C^\alpha$  atoms are indicated by the small circles (filled for a side-chain above the paper and open for a side-chain below the paper) and  $\beta$ -strips are shown as shaded regions.  $a_c$  is the distance between neighbouring  $C^\alpha$  atoms along a strand and  $b_c$  is the distance between neighbouring strands.  $\alpha$  is the angle between the strand direction and the helical axis,  $h$  is the height per turn, and  $N_T$  is the number of residues per turn which is equal to  $(p^2 + h^2)^{1/2}/a_c$ . Here the strip comprises three strands ( $m=3$ ) in an antiparallel arrangement and the whole  $\beta$ -helix comprises five strips ( $n=5$ ). The register shift between adjacent strips is four ( $t=4$ ). The register shift of the strip with itself, e.g. between strip 1 in its normal and faint depiction in the figure, is the shear number,  $s$ , and is equal to  $nt$ . In the rolled-up form  $a_c$  and  $b_c$  are helical arc distances.

### Figure 2

#### Plots of constant $d$ and $h$ in the $(nm, t/m)$ , $(nm, \alpha)$ plane and location of $\beta$ -helices and $\beta$ -barrels

Overlay of the  $(d, h)$  coordinate system at intervals of 5 Å for  $d$  (black lines) and  $h$  (red lines) on the  $(nm, t/m)$  (or  $(nm, \alpha)$ ) coordinate system for multi-strand helices with  $c=\pi$ , where  $m$  is the number of strands in the  $\beta$ -strip,  $n$  is the number of strips and  $t$  is the register shift between strips, hence  $t/m$  is the register shift per strand of the strip. Homomeric structures are indicated in blue, non-homomeric structures and  $\beta$ -strip helices in green (all with  $n=1$ ) and predicted structures in magenta. Note that not all structures have  $c=\pi$  and as such their locations in the  $(d, h)$  coordinate system are approximate. (A) Plot showing the  $\beta$ -helix and  $\beta$ -

barrel regions. **(B)**  $\beta$ -helix region showing selected  $\beta$ -helix structures from Table 2 including the transthyretin structure located using its helical dimensions ( $d_{exp}=30 \text{ \AA}$ ,  $h_{exp}=29 \text{ \AA}$ ). **(C)**  $\beta$ -barrel region showing selected  $\beta$ -barrel structures from Table 2 including the A $\beta$ (40) structure located using its helical dimensions ( $d_{exp}=28 \text{ \AA}$ ,  $\alpha_{exp}=54.4^\circ$ ).

### Figure 3

#### Plots of constant MPL in the $(nm, t/m)$ , $(nm, \alpha)$ plane.

Contours of constant MPL (kDa/nm) are shown for structures with circular cross-section, i.e.  $c=\pi$ . Contours were calculated using Eq.8 using  $m_{aa}=0.11 \text{ kDa}$ . The point shows the location of the HET-s structure (see Supplementary Result (Result.S1)).

### Figure 4

#### Transmembrane domain from $\alpha$ -haemolysin

$\alpha$ -haemolysin (PDB code: 7AHL), which incorporates seven ( $n=7$ )  $\beta$ -hairpin ( $m=2$ ) strips, each from a separate subunit. The register shift,  $t=2$ , is between equivalent strands from neighbouring  $\beta$ -hairpins and is illustrated by the alignment of highlighted residues.

### Figure 5

#### Cylindrin $\beta$ -barrel

Cylindrin(PDB code: 3SGR) comprises three ( $n=3$ )  $\beta$ -hairpins ( $m=2$ ) that form a small 6-stranded antiparallel  $\beta$ -barrel of approximately  $11 \text{ \AA}$  diameter. The barrel lacks 3-fold symmetry because the blue  $\beta$ -hairpin has the opposite orientation to the other two. The sequence has a tandem repeat. The register shift indicated by highlighted residues on the sequence and structure is two ( $t=2$ ). The highlighted residues are located on the N-terminal strand for the red and green hairpins but on the C-terminal strand for the blue hairpin.

**Figure 6****T4 phage spike  $\beta$ -helix**

The homotrimeric ( $n=3$ )  $\beta$ -helix of the T4 phage spike (PDB code: 1K28). Highlighted residues on the structure and in the sequence illustrate the register shift of eight ( $t=8$ ) between neighbouring strips (in this case a strip is a single strand,  $m=1$ ).

**Figure 7****HET-s and A $\beta$ (40) NMR structures**

(A) HET-s(218-289) molecular structure (PDB code: 2KJ3) showing both 2D and 3D representations. In the 2D representation the bold red and faint red lines show the register-shift in subunit B due to its helical conformation. This register shift is the distance between the pseudo repeat sequences denoted “N-term repeat” and “C-term repeat” in the figure. The in-register association of these two repeat sequence stabilises both the individual  $\beta$ -helices and the joins between subunits. (B) Solid state NMR structure of A $\beta$ (40) (PDB code: 2LMP) showing both 2D and 3D representations. Chains D, E and F can be regarded as continuations of chains A, B and C, respectively, through contacts made between His13 (chain  $j+3$ ) and Val40 (chain  $j$ ), as shown by the positions of their  $C^\alpha$  atoms in space-filling model. The register shift of 28 is indicated by the shift between the faint colour chain depiction and its corresponding continuing strand in bold. Thus we have a  $\beta$ -strip helix with  $n=1$ ,  $m=3$  and  $t=28$ . This arrangement allows each three-stranded  $\beta$ -strip helix to join end-to-end and in-register to form the protofilament.

**Figure 8****Geometrically correctly proportioned 3D folded-paper models of protofilament subunits**

(A) Cylindrical model of the proposed transthyretin protofilament showing the junction

between  $\beta$ -strip helices joined end-to-end by the same  $\beta$ -sheet hydrogen bonding that stabilizes the helical fold of the subunit. Print Fig.S1 and fold into both cylinder of prism models. **(B)** Prism model of the proposed A $\beta$ (40) amyloid protofilament subunit, showing the junction between  $\beta$ -strip helices joined end-to-end. Print Fig.S2 and Fig.S3 to fold into cylinder and prism models, respectively. **(C)** Proposed mechanism for amyloid protofilament subunit formation. Identical strands come together in register to form the  $\beta$ -strip. The natural tendency for a  $\beta$ -sheet to twist means that eventually the outer two strands meet and hydrogen-bond together to form the  $\beta$ -strip helix with self register-shift.

Table 1 Definition of terms

Parameter	Definition
$a_c$	Helical arc distance between consecutive $C^\alpha$ atoms on strand helix (Å)
$b_c$	Helical arc distance between consecutive $C^\alpha$ atoms on neighbour helix (Å)
$a$	Direct distance (helical chord) between consecutive $C^\alpha$ atoms on strand helix (Å)
$b$	Direct distance (helical chord) between consecutive $C^\alpha$ atoms on neighbour helix (Å)
$s$	Shear number (number of residues)
$t$	Register shift between neighbouring $\beta$ -strips (number of residues)
$m$	Number of strands in $\beta$ -strip
$n$	$n$ -fold rotational symmetry=number of $\beta$ -strips in helix
$nm$	Number of strands in helix
$t/m$	Register shift per strand of the $\beta$ -strip
$d$	Maximum spanning width of cross-section of helix (Å)
$P$	Length of perimeter of cross-section of helix (Å)
$c$	Constant relating perimeter length to width
$h$	Height per helical turn (Å)
$\alpha$	Angle between the strand direction and the helical axis (degrees)
$m_{PL}$	Mass per length (kDa/nm)
$m_{aa}$	Average mass of amino acid residue (kDa)
$N_T$	Number of residues per helical turn

Table 2 Parameters of regular  $\beta$ -barrels,  $\beta$ -helices, and amyloid fibrils

Name	PDB	<i>n</i>	<i>m</i>	<i>nm</i>	<i>t</i>	<i>s</i>	<i>t/m</i>	<i>d</i> (Å)	Par/Anti	Hollow*
<b><math>\alpha/\beta</math> barrels</b>										
Triose P Isom.	1tim	1	8	8	8	8	1.0	15	P	N
RNAse P	1v77	1	7	7	8	8	1.14	14	P	N
Ribonuc reduc.	1rlr	1	10	10	10	10	1.0	18	P(A)	N
<b>Cytoplasmic <math>\beta</math>-barrels</b>										
Asp tRNA syn.	1asy	1	5	5	8	8	1.6	12	A(P)	N
IL-1( $\beta$ -trefoil)	1l2h	1	6	6	12	12	2.0	16	A	N
EF-Tu	1efc	1	6	6	10	10	1.67	13	A	N
FMN BP	1flm	1	6	6	10	10	1.67	13	A	N
F1 ATPase	1bmf	1	6	6	8	8	1.33	12	A	N
TFIIa	1nh2	1	6	6	14	14	2.33	17	A	N
Aconitase	1aco	1	7	7	10	10	1.42	14	AP	N
Retinol BP	1rbp	1	8	8	12	12	1.5	18	A	N
Cyclophilin	1w8m	1	8	8	10	10	1.25	17	A	N
Green fluor. P	1ema	1	11	11	14	14	1.27	23	A(P)	N
<b><math>\beta</math>-helices</b>										
MfpA (PRP)	2bm5	1	1	1	20	20	20	21	P	N
Pectin lyase	1idk	1	1	1	23	23	23	23	P	N
Pman. Isomer.	1pmi	1	2	2	18	18	9.0	20	A	N
<b>Homomeric <math>\beta</math>-helices</b>										
T4 phage spike	1k28	3	1	3	8	24	8.0	25	P	N
T4 short tail fibre	1h6w	3	1	3	6	18	6.0	22	P	N
K1Fphage endosia	1v0f	3	1	3	6	18	6.0	22	P	N
<b>Trans-membrane <math>\beta</math>-barrels</b>										
OmpX	1qj9	1	8	8	8	8	1.0	15	A	Y
OmpA	1bxw	1	8	8	10	10	1.2	20	A	Y
OmpT	1i78	1	10	10	12	12	1.2	25	A	Y
OpcA	1k24	1	10	10	12	12	1.2	25	A	Y
FadL	3dwo	1	12	12	14	14	1.16	27	A	Y
Omp32	2fgr	1	16	16	20	20	1.27	33	A	Y
Porin	2omf	1	16	16	20	20	1.27	33	A	Y
Maltoporin	1mpm	1	18	18	22	22	1.22	37	A	Y
FhuA (TonB)	1by5	1	22	22	22	22	1.0	42	A	Y
FepA (TonB)	1fep	1	22	22	24	24	1.09	43	A	Y
<b>Homomeric trans-membrane <math>\beta</math>-barrels</b>										
$\alpha$ -haemolysin	7ahl	7	2	14	2	14	1.0	26	A	Y
$\gamma$ -haemolysin	3b07	4	4	16	4	16	1.0	30	A	Y
Mycobact. OM Channel MspA	1uun	8	2	16	4	32	2.0	41	A	Y
		8	2	16	2	16	1.0	30	A	Y
TolC	1ek9	3	4	12	8	24	2.0	31	A	Y
Adhesin Hia	2gr7	3	4	12	4	12	1.0	22	A	N
CsgG	3x2r	9	4	36	2	18	0.5	59	A	Y
<b>Homomeric cytoplasmic <math>\beta</math>-barrels</b>										
Cylindrin	3sgr	3	2	6	2	6	1.0	12	A	N
RUBISCO	1bxn	4	2	8	2	8	1.0	15	A	N
Muconolact. Isom.	3zo7	2	4	8	6	12	1.5	17	A	N
GTP cyclohydrol.	1gtp	5	4	20	4	20	1.0	37	A	N
<b>Amyloid fibrils, putative amyloid structures</b>										
A $\beta$ (40) NMR	2lmp	1	3	3	28	28	9.3	32-37	P	N
HET-s	2rnm	1	1	1	36	36	36	38	P	N
Transthyr. amyloid	&	1	6	6	28	28	4.7	30	P	N
A $\beta$ (40) amyloid	&	1	10	10	20	20	2.0	28	P	N

$\alpha$ -nanotube	£	1	9	9	18	18	2.0	23	P	N
Perutz $\beta$ -helix	\$	1	1	1	20	20	20	20	P	N

Homomeric structures with  $n$ -fold ( $n > 1$ ) rotational symmetry are in shaded regions. Possible exceptions are cylindrin, where one of the three  $\beta$ -hairpins points in the opposite direction to the others, and the triple-strand  $\beta$ -helices which exhibit minor deviations from 3-fold symmetry.  $m$  is the number of strands in the  $\beta$ -strip.  $nm$  gives the number of strands in the multi-strand helix.  $t$  is the register shift per  $\beta$ -strip.  $t/m$  is the register shift per strand of the  $\beta$ -strip.  $s$  is the shear number.  $d$  is the helix diameter, in Å.

\*Hollow proteins have a water-filled cavity centred on the helical axis that is involved in membrane transport. In gram-negative bacteria they are typically situated in the outer membrane (OM).

All barrels and  $\beta$ -helices listed have continuous hydrogen bonding joining adjacent strands. If an amino acid lacking any appropriate inter-strand hydrogen bonding occurs as a link in the continuous hydrogen bonding, such a barrel is rejected.

<sup>&</sup>Parameters calculated from dimensions derived from fibre diffraction studies.

<sup>†</sup>Parameters from amyloid fibre model proposed earlier<sup>26</sup>.

<sup>‡</sup>Parameters from amyloid fibre model proposed earlier<sup>39</sup>.

Note the structure of the non-homeric lipopolysaccharide transport protein, LptD, has not been included as it appears to be an unusual hybrid of two  $\beta$ -barrels each with a different barrel width and shear number.

**Table 3 Measured and modelled parameter values for transthyretin and A $\beta$ (40)**

	x-section	$d_{exp}$	$h_{exp}$	$\alpha_{exp}$	$nm$	$t/m$	$nm_{mod}$	$t/m_{mod}$	$n_{mod}$	$m_{mod}$	$t_{mod}$	$d_{mod}$	$h_{mod}$	$\alpha_{mod}$
<b>Transthyretin</b>	Triangle	30.0	29.0	-	5.8	4.5	6	4.67	1	6	28	32.3	30.2	72.7
	Circle				5.8	4.7	6	4.67	1	6	28	30.8	30.2	72.7
<b>A<math>\beta</math>(40)</b>	Triangle	28.0	-	54.4	10.4	1.99	10	2.0	1	10	20	27.0	57.7	54.5
	Circle				10.9	1.99	11	2.0	1	11	22	28.4	63.5	54.5

The values for  $d_{exp}$  and  $h_{exp}$  or  $\alpha_{exp}$  are from fiber X-ray fibre diffraction experiments and are measured in Å and degrees, respectively.

Calculations using Eq.1a and Eq.2 yield  $nm$  and  $t/m$ , which are adjusted to  $nm_{mod}$  and  $t/m_{mod}$  such that  $nm$  is an integer and  $s=nm \times t/m$  is equal to the nearest even integer. Eq.3 are then used to determine,  $d_{mod}$  and  $h_{mod}$ . Results are given for both multi-strand helices of triangular and circular cross-section. Two modelled structures are depicted in Fig.8.

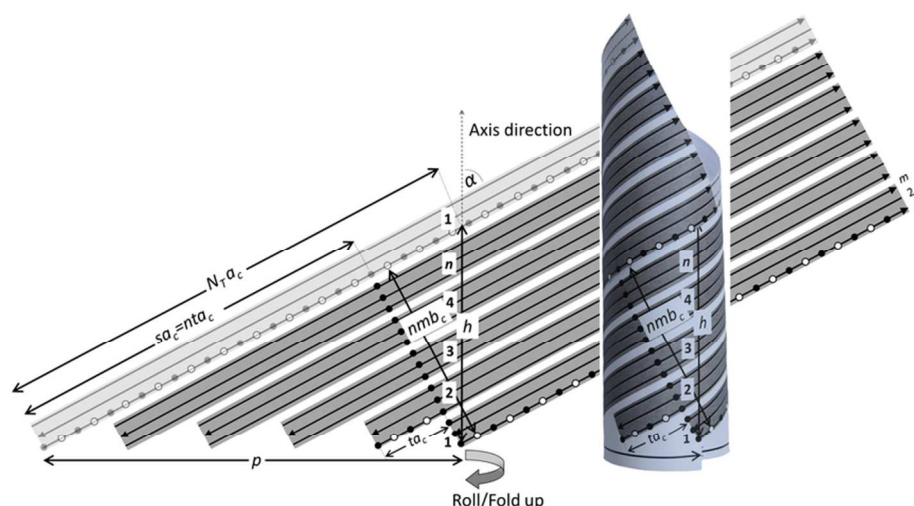


Figure 1. Schematic showing geometry in 2D and 3D forms of a general multi-strand helix. Depiction of an unrolled/unfolded 2D form of a multi-strand helix of any general cross-sectional shape with perimeter length  $p$  and rolled-up cylinder form. Ca atoms are indicated by the small circles (filled for a side-chain above the paper and open for a side-chain below the paper) and  $\beta$ -strips are shown as shaded regions.  $a_c$  is the distance between neighbouring Ca atoms along a strand and  $b_c$  is the distance between neighbouring strands.  $\alpha$  is the angle between the strand direction and the helical axis,  $h$  is the height per turn, and  $N_T$  is the number of residues per turn which is equal to  $(p^2 + h^2)^{1/2} / a_c$ . Here the strip comprises three strands ( $m=3$ ) in an antiparallel arrangement and the whole  $\beta$ -helix comprises five strips ( $n=5$ ). The register shift between adjacent strips is four ( $t=4$ ). The register shift of the strip with itself, e.g. between strip 1 in its normal and faint depiction in the figure, is the shear number,  $s$ , and is equal to  $N_T$ . In the rolled-up form  $a_c$  and  $b_c$  are helical arc distances."

40x22mm (600 x 600 DPI)

Accep



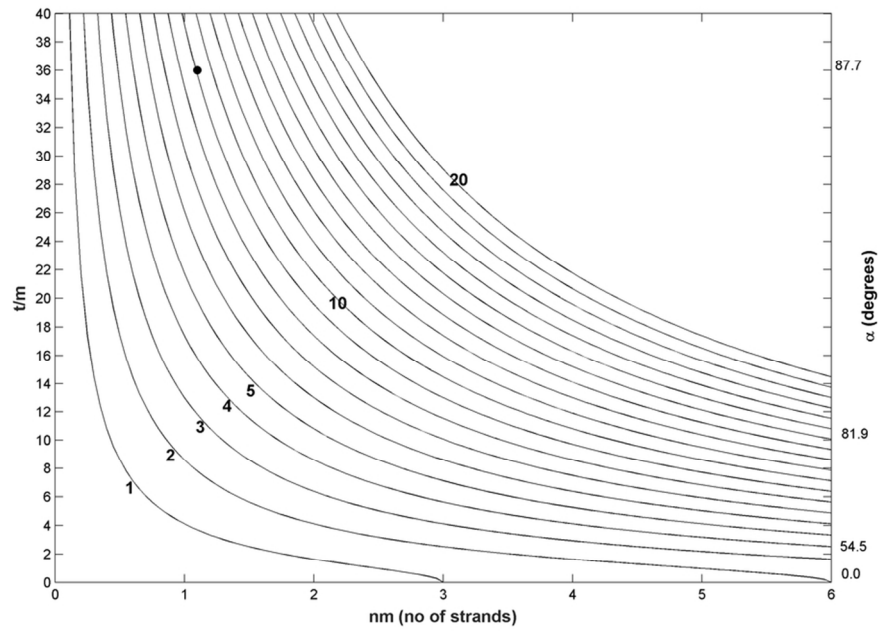


Figure 3. **Plots of constant MPL in the (nm,t/m), (nm, $\alpha$ ) plane.** Contours of constant MPL (kDa/nm) are shown. Contours were calculated using Eq.8 using  $m_{aa}=0.11$  kDa. The point shows the location of the HET-s structure (see Supplementary Result (Result.S1)).

44x30mm (600 x 600 DPI)

Accept

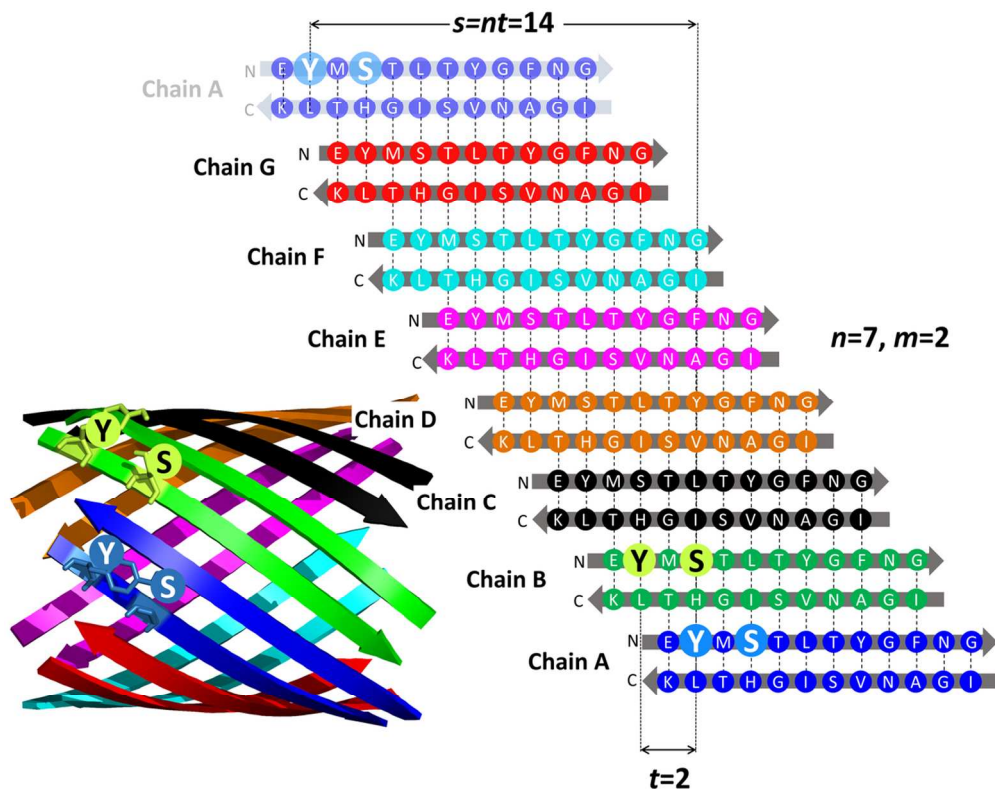


Figure 4. **Transmembrane domain from  $\alpha$ -haemolysin.**  $\alpha$ -haemolysin (PDB code: 7AHL), which incorporates seven ( $n=7$ )  $\beta$ -hairpin ( $m=2$ ) strips, each from a separate subunit. The register shift,  $t=2$ , is between equivalent strands from neighbouring  $\beta$ -hairpins and is illustrated by the alignment of highlighted residues.

114x90mm (300 x 300 DPI)

Accel

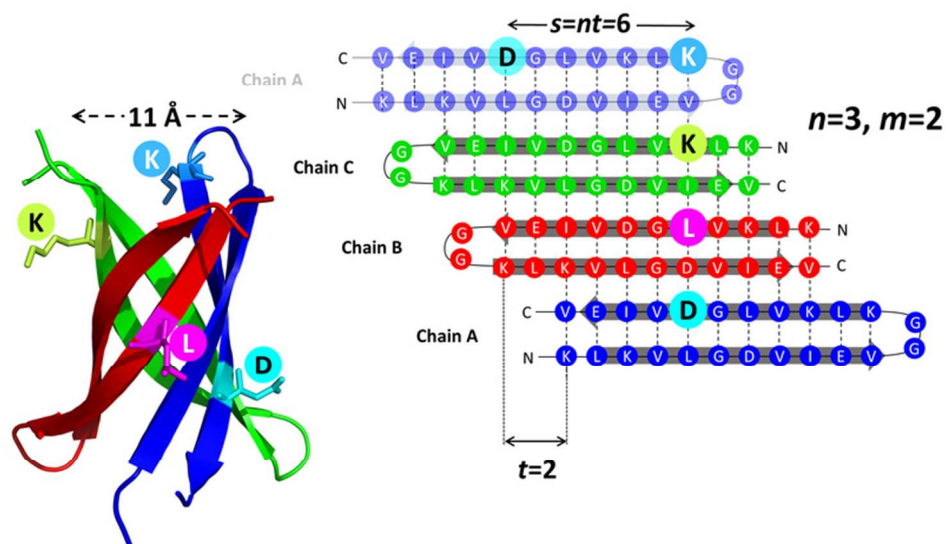


Figure 5. **Cylindrin  $\beta$ -barrel.** Cylindrin (PDB code: 3SGR) comprises three ( $n=3$ )  $\beta$ -hairpins ( $m=2$ ) that form a small 6-stranded antiparallel  $\beta$ -barrel of approximately 11 Å diameter. The barrel lacks 3-fold symmetry because the blue  $\beta$ -hairpin has the opposite orientation to the other two. The sequence has a tandem repeat. The register shift indicated by highlighted residues on the sequence and structure is two ( $t=2$ ). The highlighted residues are located on the N-terminal strand for the red and green hairpins but on the C-terminal strand for the blue hairpin.

71x40mm (300 x 300 DPI)

Accept

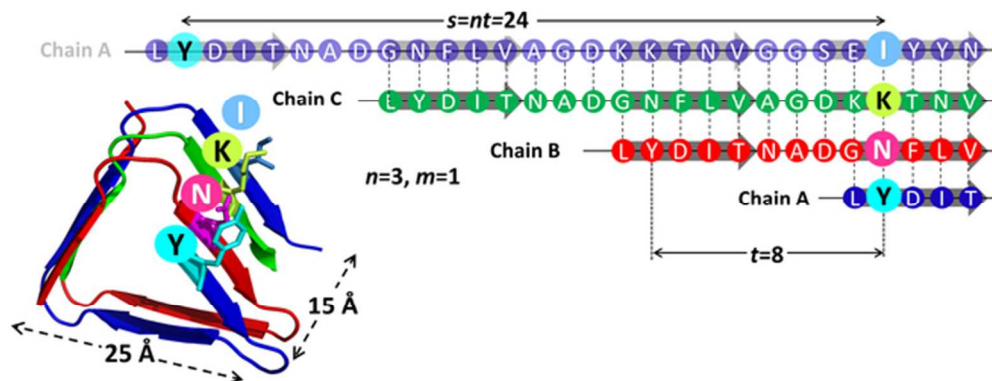


Figure 6. **T4 phage spike  $\beta$ -helix.** The homotrimeric ( $n=3$ )  $\beta$ -helix of the T4 phage spike (PDB code: 1K28). Highlighted residues on the structure and in the sequence illustrate the register shift of eight ( $t=8$ ) between neighbouring strips (in this case a strip is a single strand,  $m=1$ ).

55x23mm (300 x 300 DPI)

Accepted

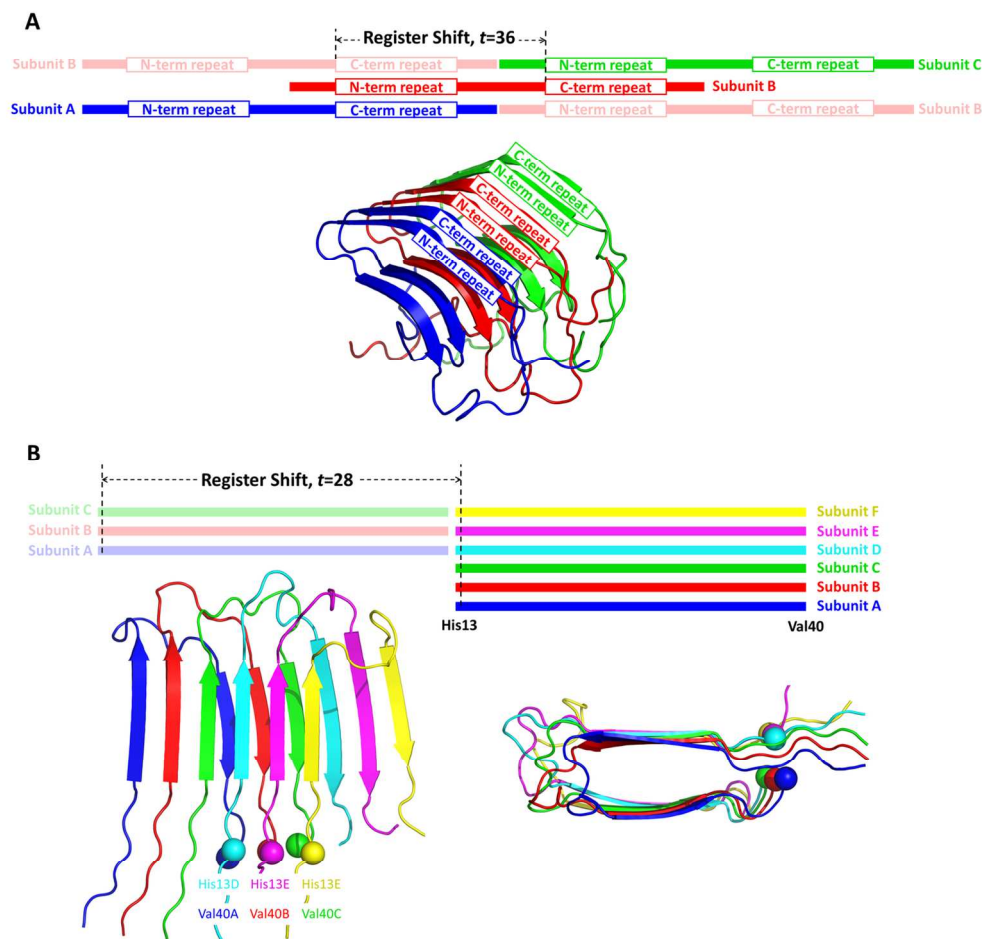


Figure 7. **HET-s and A $\beta$ (40) NMR structures.** (A) HET-s(218-289) molecular structure (PDB code: 2KJ3) showing both 2D and 3D representations. In the 2D representation the bold red and faint red lines show the register-shift in subunit B due to its helical conformation. This register shift is the distance between the pseudo repeat sequences denoted "N-term repeat" and "C-term repeat" in the figure. The in-register association of these two repeat sequence stabilises both the individual  $\beta$ -helices and the joins between subunits. (B) Solid state NMR structure of A $\beta$ (40) (PDB code: 2LMP) showing both 2D and 3D representations. Chains D, E and F can be regarded as continuations of chains A, B and C, respectively, through contacts made between His13 (chain  $j+3$ ) and Val40 (chain  $j$ ), as shown by the positions of their Ca atoms in space-filling model. The register shift of 28 is indicated by the shift between the faint colour chain depiction and its corresponding continuing strand in bold. Thus we have a  $\beta$ -strip helix with  $n=1$ ,  $m=3$  and  $t=28$ . This arrangement allows each three-stranded  $\beta$ -strip helix to join end-to-end and in-register to form the protofilament.

128x128mm (300 x 300 DPI)

A

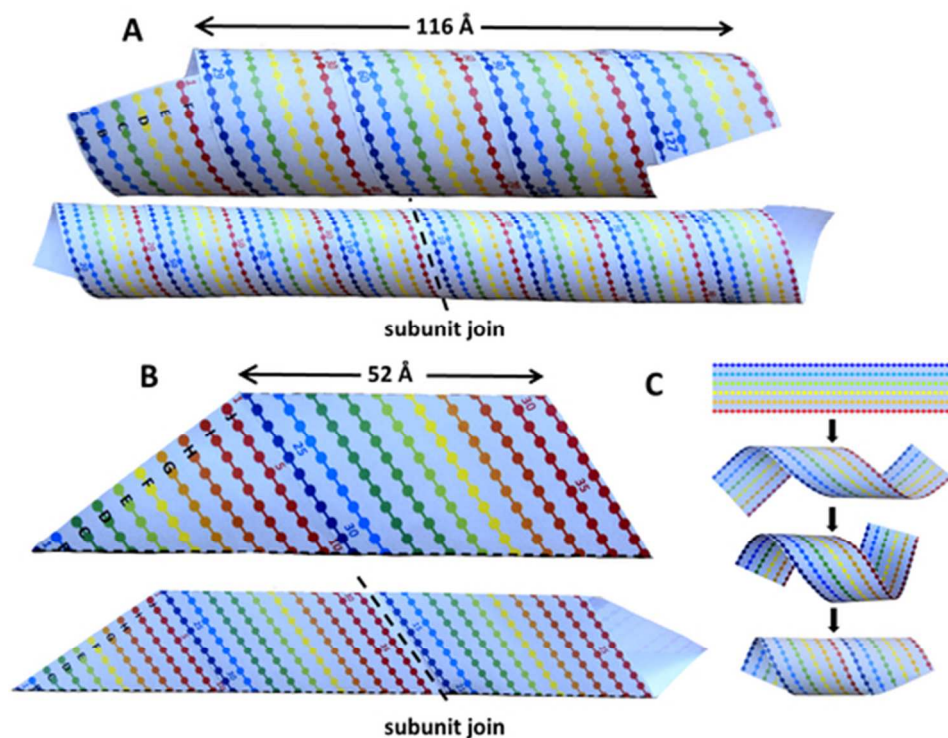


Figure 8. **Geometrically correctly proportioned 3D folded-paper models of protofilament subunits.**

(A) Cylindrical model of the proposed transthyretin protofilament showing the junction between  $\beta$ -strip helices joined end-to-end by the same  $\beta$ -sheet hydrogen bonding that stabilizes the helical fold of the subunit. Print Fig.S1 and fold into both cylinder of prism models. (B) Prism model of the proposed  $A\beta(40)$  amyloid protofilament subunit, showing the junction between  $\beta$ -strip helices joined end-to-end. Print Fig.S2 and Fig.S3 to fold into cylinder and prism models, respectively. (C) Proposed mechanism for amyloid protofilament subunit formation. Identical strands come together in register to form the  $\beta$ -strip. The natural tendency for a  $\beta$ -sheet to twist means that eventually the outer two strands meet and hydrogen-bond together to form the  $\beta$ -strip helix with self register-shift.

48x35mm (300 x 300 DPI)

Acce